A Study on Scattering Performance of Reflectarray Element Covered by Dielectric Superstrate

Keisuke Konno, *Member, IEEE*, and Qiang Chen, *Senior Member, IEEE*

***Abstract*— In this article, effect of a dielectric superstrate on scattering performance of reflectarray elements is clarified. At first, analytical electric field expressions of an infinite line current backed by a ground plane with the dielectric superstrate and so-called resonance conditions derived by Sugio *et al.*, are reviewed. According to the electric field expressions and reciprocity, enhancement of the scattering field strength by the dielectric superstrate under the resonance conditions is expressed analytically. Since the scatterers are illuminated by the incident wave arriving from outside of the scatterers, the effect of its incident angle θ_i on the scattering field strength is also studied. Based on inequalities that are derived from the electric field expressions, range of θ_i for enhancing the scattering field strength by the dielectric superstrate under the resonance conditions is found. As a result, it is found that the range of θ_i is independent of ε_r when $\varepsilon_r \gg 1$, where ε_r is relative permittivity of the dielectric superstrate. Numerical simulation is performed, and it is demonstrated that the analytical formulae derived here are useful for predicting the effect of the dielectric superstrate on practical reflect array elements such as dipole, patch, and loop elements. Results and theories demonstrated in this article give quantitative guidelines on designing the reflectarray elements covered by the superstrate from the viewpoints of angle dependence, geometry, and permittivity of the superstrate.**

***Index Terms*— Reflectarray, scatterer, superstrate.**

I. Introduction

IT IS well-known that a dielectric superstrate is a kind of spatial filter and can enhance the performance of antennas such as gain. Sugio *et al.* [1]–[3] have derived that electric field strength of the antennas can be enhanced by the dielectric superstrate. In the studies, expressions of the electric field from an infinite line current over a ground plane with the dielectric superstrate have been derived analytically. According to the derived expressions, it has been demonstrated that the electric field strength of the infinite line current over a ground plane is proportional to $\sqrt{\varepsilon_r}$ when its geometry is optimized so that its main beam is directed to the broadside direction. Moreover, the optimized geometry has been demonstrated, i.e., $h = (\lambda_0/2)$ and $t = (\lambda_0/(4\sqrt{\varepsilon_r}))$, where h is height of the dielectric superstrate from the ground plane, t is the thickness of the dielectric superstrate, and λ_0 is wavelength in free-space. Detailed studies on the dielectric (and magnetic) superstrate and its effect on radiation performance of the antennas have also been demonstrated by Alexópoulos and Jackson [4]–[6]. For example, effect of multiple layers of the dielectric (and magnetic) superstrate on radiation performance of the antennas has been demonstrated [7]. Moreover, microstrip scatterers covered by the dielectric superstrate have been studied [8]. It has been demonstrated that radiation efficiency of the scatterers affect their radar cross section (RCS). The antennas covered by the superstrate are called as Fabry–Pérot cavity antennas or resonant cavity antennas.

Based on these pioneering works on the Fabry–Pérot cavity antennas, numerous Fabry–Pérot cavity antennas have been proposed [9]–[20]. Low profile Fabry–Pérot cavity antennas have been proposed using an electromagnetic band gap (EBG) superstrate [9] or an artificial magnetic conductor (AMC) ground plane, respectively [10]. Broadband or dual band Fabry–Pérot cavity antennas have been developed using the superstrate covered by a frequency selective surface (FSS) [11], [15]. Radiation performance of the Fabry–Pérot cavity antennas have been enhanced. For example, it has been demonstrated that antenna gain of the Fabry–Pérot cavity antenna can be enhanced using perforated dielectric superstrates [16]. A Fabry–Pérot cavity antenna using a truncated dielectric superstrate has been proposed and its cosecant-squared radiation pattern has been demonstrated [19]. A beam steering ability of the Fabry–Pérot cavity antennas using a metamaterial-based superstrate has been demonstrated [13]. The Fabry–Pérot cavity antennas using active components have been proposed and their beam scanning capability have been demonstrated experimentally [12], [13].

On the other hand, so-called reflectarrays have been studied so far [21]–[23]. The reflectarrays are reflector antennas and their reflecting surface is composed of scattering elements. For example, design method of reflectarrays [24]–[28], 3-D-printed reflectarrays, and related technologies have been proposed in previous studies [29]–[37]. The reflectarrays covered by the superstrate have been proposed and some of them are called as folded reflectarray [38]–[50]. The superstrate of the folded reflectarray works as a polarizer and is located at a distance equal to half of the focal length of the reflectarray. The polarizer scatters an incident wave from a primary source which is integrated with the reflecting surface and the reflecting surface is illuminated. The reflecting surface twists

Manuscript received 27 January 2022; revised 10 April 2022; accepted 28 May 2022. Date of publication 24 June 2022; date of current version 9 November 2022. This work was supported in part by the Ministry of Internal Affairs and Communications in Japan under Grant JPJ000254. *(Corresponding author: Keisuke Konno.)*

The authors are with the Department of Communications Engineering, Graduate School of Engineering, Tohoku University, Sendai 980-8577, Japan (e-mail: konno@ecei.tohoku.ac.jp).

Color versions of one or more figures in this article are available at https://doi.org/10.1109/TAP.2022.3184526.

Digital Object Identifier 10.1109/TAP.2022.3184526

the polarization and its scattering wave passes through the polarizer. As a result, the total height of the folded reflectarray including spacing between the primary source and the reflecting surface can be reduced to half of the reflectarray without the polarizer. The folded reflectarray has been enhanced for broadband or dual-band operation [42], [44], [46], [47] and beam scanning [45], [49]. Moreover, the folded reflectarray with a conformal polarizer [47] or a substrate integrated waveguide (SIW) polarizer [48] have been developed.

Although numerous works on antennas or scatterers covered by the superstrate have been found, effect of the dielectric superstrate on the scattering performance of the reflectarrays or reflectarray elements has not been clarified yet. Meriah *et al.* [51] has performed parametric studies and demonstrated that the dielectric superstrate can enhance the gain of the reflectarray. However, the optimum geometry of the dielectric superstrate for enhancing the electric field strength of the reflectarray element has not been clarified in this work due to lack of theoretical discussion. In addition, effect of the incident angle on the scattering field strength of the reflectarray element has not been discussed in this work. Therefore, it can be said that potential application of the dielectric superstrate to enhance the performance of scatterers such as reflectarrays has been unclear so far because its theoretical study is absent. The dielectric superstrate is easily applicable to reflectarrays working at high-frequency band such as millimeter waveband because its physical thickness is small. Once the effect of the dielectric superstrate on the performance of the scatterers is clarified, a new horizon of the reflectarray covered by the dielectric superstrate can be explored for the next-generation wireless systems. Therefore, the effect of the dielectric superstrate on the scattering performance of the reflectarray element is expected to be clarified theoretically in advance of designing the reflectarrays covered by the dielectric superstrate working at the high-frequency band.

In this article, the effect of the superstrate on the scattering field strength of the reflectarray element is clarified theoretically. At first, the analytical expressions on the far-field of the infinite line current and so-called resonance conditions derived by Sugio *et al.* [1]–[3] are reviewed. According to the expressions and reciprocity, it is demonstrated that the scattering field strength of the infinite line scatterer illuminated by the plane wave of normal incidence is proportional to ϵ_r under the resonance conditions in backscattering direction. Moreover, range of the incident angle θ_i for enhancing the scattering field strength by the dielectric superstrate under the resonance conditions is found to be independent of ϵ_r when $\epsilon_r \gg 1$. Next, a couple of finite reflectarray elements covered by the dielectric superstrate are modeled and their scattering performances are simulated using the method of moments (MoM). It is demonstrated that the derived theories in this article work for the practical reflectarray elements. Finally, phase variation of reflection coefficient of the practical reflectarray elements is numerically obtained and the effect of the superstrate on it is discussed.

This article is organized as follows. The analytical expressions on the far-field of the infinite line current and resonance conditions derived by Sugio *et al.* [1]–[3] are reviewed in Section II. Effect of the incident angle θ_i on the scattering field strength of the infinite line scatterer covered by the superstrate under the resonance conditions is clarified in Section III. In order to demonstrate the effectiveness of the derived theory, numerical simulation of a couple of finite reflectarray elements covered by the dielectric superstrate is performed by the MoM in Section IV. Finally, this article is concluded in Section V.

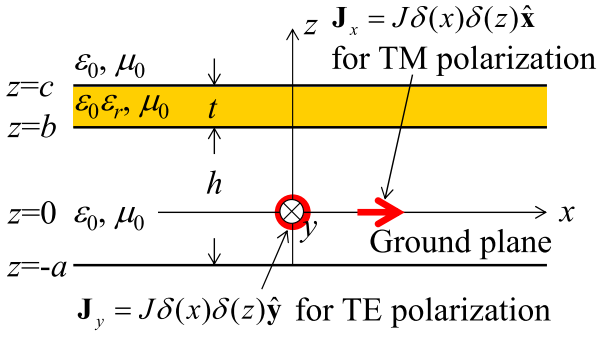

Fig. 1. Infinite line current backed by ground plane with dielectric superstrate.

II. Analytical Study

Here, analytical electric field expressions of the infinite line current backed by the ground plane with the dielectric superstrate are reviewed [1]–[3]. Fig. 1 shows the infinite line current along the y-axis backed by the ground plane with the dielectric superstrate. Since the line current is infinitely long along the y-axis, the electric fields are independent of y and are obtained from following 2-D wave equations:

$$\frac{\partial^2 E_y}{\partial x^2} + \frac{\partial^2 E_y}{\partial z^2} + k^2 E_y = j\omega\mu_0 J\delta(x)\delta(z) \tag{1}$$

$$\frac{\partial^2 E_x}{\partial x^2} + \frac{\partial^2 E_x}{\partial z^2} + k^2 E_x = j\omega\mu_0 J\delta(x)\delta(z) \tag{2}$$

where $k = k_0(=\omega\sqrt{\varepsilon_0\mu_0})$ when $-a \le z \le b$, $c \le z$ while $k = k_0\sqrt{\varepsilon_r}$ when $b \le z \le c$. J is current, ω is angular frequency, and μ_0 is permeability of free-space. Equation (1) is for TE polarization and (2) is for TM polarization, respectively. Rigorous electric field expressions of the infinite line current backed by the ground plane with the dielectric superstrate are obtained from (1) and (2) once the Fourier transform is applied to them. Finally, a saddle point method is applied to the rigorous electric field expressions and far-field expressions of the infinite line current backed by the ground plane with the dielectric superstrate are readily obtained. The far-field expressions obtained from (1) are as follows:

$$E_\phi^{\mathrm{TE}}(\theta, h, t, \varepsilon_r, a) = \frac{-j\omega\mu_0 J}{\sqrt{2\pi k_0\rho}} \frac{e^{-j(k_0\rho-\pi/4)} E_0^{\mathrm{TE}}(\theta, a)}{F^{\mathrm{TE}}(\theta, h, t, \varepsilon_r)} \tag{3}$$

$$E_0^{\mathrm{TE}}(\theta, a) = \sin(k_0 a\cos\theta) \tag{4}$$

where ρ is radial distance of the cylindrical coordinates. The far-field expressions obtained from (2) are as follows:

$$E_\theta^{\mathrm{TM}}(\theta, h, t, \varepsilon_r, a) = \frac{-\omega\mu_0 J}{\sqrt{2\pi k_0\rho}} \frac{e^{-j(k_0\rho-\pi/4)} E_0^{\mathrm{TM}}(\theta, a)}{F^{\mathrm{TM}}(\theta, h, t, \varepsilon_r)} \tag{5}$$

$$E_0^{\mathrm{TM}}(\theta, a) = \sin(k_0 a\cos\theta)\cos\theta. \tag{6}$$

Here, F^{TE} and F^{TM} are as follows:

$$F^{\mathrm{TE}}(\theta,h,t,\varepsilon_r) = \cos(k_0t\xi)e^{jk_0h\cos\theta} + j\sin(k_0t\xi) \times\left\{\frac{\cos\theta}{\xi}\cos(k_0h\cos\theta) + j\frac{\xi}{\cos\theta}\sin(k_0h\cos\theta)\right\} \quad (7)$$

$$F^{\mathrm{TM}}(\theta,h,t,\varepsilon_r) = \cos(k_0t\xi)e^{jk_0h\cos\theta} + \sin(k_0t\xi) \times\left\{\frac{\xi}{j\varepsilon_r\cos\theta}\cos(k_0h\cos\theta) + \frac{\varepsilon_r\cos\theta}{\xi}\sin(k_0h\cos\theta)\right\} \quad (8)$$

$$\xi = \sqrt{\varepsilon_r - \sin^2\theta}. \quad (9)$$

As shown in (4) and (6), E_0^{TE} and E_0^{TM} are corresponding to TE and TM polarization of far-fields of an infinitesimal dipole element backed by the ground plane, respectively (i.e., E_0^{TE} and E_0^{TM} are E_ϕ and E_θ in xz-plane, respectively). Therefore, it is found that effect of the superstrate on the electric field strength of the infinite line current backed by the ground plane with the dielectric superstrate is included in F^{TE} and F^{TM}. According to (7) and (8), thickness of the superstrate ($=t$) and spacing between the superstrate and the ground plane ($=h$) for maximizing magnitude of E_ϕ^{TE} and E_θ^{TM} in θ direction are obtained as follows:

$$h_{(m,\theta)} = \frac{m\lambda_0}{2\cos\theta} \quad \text{where} \quad m = 1,2,\ldots \quad (10)$$

$$t_{(n,\theta)} = \frac{(2n-1)\lambda_0}{4\sqrt{\varepsilon_r - \sin^2\theta}} \quad \text{where} \quad n = 1,2,\ldots \quad (11)$$

Equations (10) and (11) are well-known as so-called resonance conditions. Relative electric field strength of the infinite line current backed by the ground plane with the dielectric superstrate can be expressed as follows when the resonance conditions given by (10) and (11) are satisfied:

$$\left|\frac{E_\phi^{\mathrm{TE}}(\theta,h_{(m,\theta)},t_{(n,\theta)},\varepsilon_r)}{E_0^{\mathrm{TE}}(\theta,a)}\right| = \left|\frac{\sqrt{\varepsilon_r-\sin^2\theta}}{\cos\theta}\right| \quad (12)$$

$$\left|\frac{E_\theta^{\mathrm{TM}}(\theta,h_{(m,\theta)},t_{(n,\theta)},\varepsilon_r)}{E_0^{\mathrm{TM}}(\theta,a)}\right| = \left|\frac{\varepsilon_r\cos\theta}{\sqrt{\varepsilon_r-\sin^2\theta}}\right|. \quad (13)$$

Equations (12) and (13) indicate that the electric field strength of the infinite line current backed by the ground plane can be enhanced by the dielectric superstrate and is $\sqrt{\varepsilon_r}$ times larger than that without the dielectric superstrate in broadside direction (i.e., $\theta = 0$) when the resonance conditions are satisfied.

Here, all the equations are formulated under the assumption that the space between the ground plane and the superstrate is free-space. On the other hand, general form of the equations including the medium between the ground plane and the superstrate is available, and effect of the superstrate on the radiation field strength has been demonstrated [5].

III. Range of Incident Angle for Enhancing Scattering Field Strength

Although the resonance conditions and the electric field expressions have been applied to design of numerous antennas covered by the superstrate, a couple of problems should be solved in advance of their application to the design of the scatterers covered by the dielectric superstrate. One of the biggest differences between antenna design and scatterer design is their excitation. The scatterer is illuminated by an incident wave arriving from a specific angle while the antenna is excited using voltage source connected with its port. According to reciprocity, it is easily found that the applied voltage by the incident wave is proportional to $(1/F^{\mathrm{TE/TM}})$ for the infinite line scatterer backed by the ground plane with the dielectric superstrate. Therefore, the current J in (3) and (5) is proportional to $(1/F^{\mathrm{TE/TM}})$ for scattering problem. For example, J is proportional to $\sqrt{\varepsilon_r}$ when the resonance conditions are satisfied for $\theta = 0$ and the incident wave arrives from $\theta = 0$. As a result, the scattering field strength of the infinite line scatterer backed by the ground plane with the dielectric superstrate is proportional to ε_r at $\theta = 0$ because the effect of the superstrate is squared. On the other hand, the applied voltage by the incident wave arriving from $\theta(\neq 0)$ can be reduced when the incident angle is away from $\theta = 0$. Therefore, the incident angle $\theta = \theta_i$ for enhancing scattering field strength of the infinite line scatterer backed by the ground plane with the dielectric superstrate is restricted once the resonance conditions are satisfied for specific scattering angle $\theta = \theta_s$. Here, a couple of formulae indicating the range of the incident angle $\theta = \theta_i$ for enhancing the scattering field strength are derived.

Here, the infinite line scatterer backed by the ground plane with the dielectric superstrate is illuminated by a plane wave arriving from $\theta = \theta_i$. Geometry of the superstrate is given so that resonance conditions for a specific scattering angle $\theta = \theta_s$ are satisfied, i.e., $h = h_{(1,\theta_s)}$, $t = t_{(1,\theta_s)}$. The superstrate is made of lossless dielectric material.

A. TE Incidence

According to (3) and (4), the range of the incident angle θ_i for enhancing the scattering field strength can be obtained from following inequality:

$$\left|\frac{E_0^{\mathrm{TE}}(\theta_s,a)}{F^{\mathrm{TE}}(\theta_s,h_{(1,\theta_s)},t_{(1,\theta_s)},\varepsilon_r)}\frac{E_0^{\mathrm{TE}}(\theta_i,a)}{F^{\mathrm{TE}}(\theta_i,h_{(1,\theta_s)},t_{(1,\theta_s)},\varepsilon_r)}\right| \geq \left|E_0^{\mathrm{TE}}(\theta_s,a)E_0^{\mathrm{TE}}(\theta_i,a)\right|. \quad (14)$$

Here, it should be noted that the resonance conditions for the scattering angle $\theta = \theta_s$ are satisfied (i.e., $h = h_{(1,\theta_s)}$, $t = t_{(1,\theta_s)}$). Substituting (12) into (14), (14) can be simplified as follows:

$$\left|F^{\mathrm{TE}}(\theta_i,h_{(1,\theta_s)},t_{(1,\theta_s)},\varepsilon_r)\right|^2 \leq \frac{\varepsilon_r-\sin^2\theta_s}{\cos^2\theta_s}. \quad (15)$$

The range of the incident angle θ_i can be exactly obtained once (15) is solved using nonlinear solvers. On the other hand, (15) can be approximated and a simplified expression is derived when $\varepsilon_r \gg 1$. According to (9) and (11), $k_0t_{(1,\theta_s)}\xi$

can be approximated as follows:

$$k_0 t_{(1,\theta_s)}\xi = \frac{2\pi}{\lambda_0}\frac{(2-1)\lambda_0}{4\sqrt{\varepsilon_r-\sin^2\theta_s}}\sqrt{\varepsilon_r-\sin^2\theta_i} \approx \frac{\pi}{2} \quad \left(\because \frac{\sqrt{\varepsilon_r-\sin^2\theta_i}}{\sqrt{\varepsilon_r-\sin^2\theta_s}} \approx 1\right). \tag{16}$$

Once (16) is substituted into (7) and $\varepsilon_r \gg 1$ is used, the left-hand side of (15) can be approximated as follows:

$$\begin{aligned}\left|F^{\mathrm{TE}}(\theta_i, h_{(1,\theta_s)}, t_{(1,\theta_s)}, \varepsilon_r)\right|^2 &\approx \frac{\cos^2\theta_i}{\varepsilon_r-\sin^2\theta_i}\cos^2(k_0 h_{(1,\theta_s)}\cos\theta_i) \\ &\quad + \frac{\varepsilon_r-\sin^2\theta_i}{\cos^2\theta_i}\sin^2(k_0 h_{(1,\theta_s)}\cos\theta_i) \\ &\approx \frac{\varepsilon_r}{\cos^2\theta_i}\sin^2(k_0 h_{(1,\theta_s)}\cos\theta_i).\end{aligned} \tag{17}$$

Finally, the left-hand side of (15) is approximated by (17) and the right-hand side of (15) is approximated as $(\varepsilon_r - \sin^2\theta_s)/(\cos^2\theta_s) \approx (\varepsilon_r/(\cos^2\theta_s))$, following inequality is obtained:

$$\sin^2(k_0 h_{(1,\theta_s)}\cos\theta_i) \le \frac{\cos^2\theta_i}{\cos^2\theta_s}. \tag{18}$$

Since ε_r is not included in (18), it is found that the range of the incident angle θ_i for enhancing the scattering field strength of the infinite line current backed by the ground plane with the dielectric superstrate is independent of ε_r when $\varepsilon_r \gg 1$.

B. TM Incidence

According to (5) and (6), the range of the incident angle θ_i for enhancing the scattering field strength can be obtained from following inequality:

$$\left|\frac{E_0^{\mathrm{TM}}(\theta_s, a)}{F^{\mathrm{TM}}(\theta_s, h_{(1,\theta_s)}, t_{(1,\theta_s)}, \varepsilon_r)}\frac{E_0^{\mathrm{TM}}(\theta_i, a)}{F^{\mathrm{TM}}(\theta_i, h_{(1,\theta_s)}, t_{(1,\theta_s)}, \varepsilon_r)}\right| \ge \left|E_0^{\mathrm{TM}}(\theta_s, a)E_0^{\mathrm{TM}}(\theta_i, a)\right|. \tag{19}$$

Here, it should be noted that the resonance conditions for the scattering angle $\theta = \theta_s$ are satisfied (i.e., $h = h_{(1,\theta_s)}, t = t_{(1,\theta_s)}$) in the same manner as the TE incidence. Substituting (13) into (19), (19) can be simplified as follows:

$$\left|F^{\mathrm{TM}}(\theta_i, h_{(1,\theta_s)}, t_{(1,\theta_s)}, \varepsilon_r)\right|^2 \le \frac{\varepsilon_r^2\cos^2\theta_s}{\varepsilon_r-\sin^2\theta_s}. \tag{20}$$

The range of the incident angle θ_i can be exactly obtained once (20) is solved using nonlinear solvers. In the same manner as the TE incidence, (20) can be approximated and a simplified expression is derived when $\varepsilon_r \gg 1$. Equation (16) is substituted into (8) and $\varepsilon_r \gg 1$ is used, the left-hand side of (20) can be approximated as follows:

$$\begin{aligned}\left|F^{\mathrm{TM}}(\theta_i, h_{(1,\theta_s)}, t_{(1,\theta_s)}, \varepsilon_r)\right|^2 &\approx \frac{\varepsilon_r-\sin^2\theta_i}{\varepsilon_r^2\cos^2\theta_i}\cos^2(k_0 h_{(1,\theta_s)}\cos\theta_i) \\ &\quad + \frac{\varepsilon_r^2\cos^2\theta_i}{\varepsilon_r-\sin^2\theta_i}\sin^2(k_0 h_{(1,\theta_s)}\cos\theta_i) \\ &\approx \varepsilon_r\cos^2\theta_i\sin^2(k_0 h_{(1,\theta_s)}\cos\theta_i).\end{aligned} \tag{21}$$

Finally, the left-hand side of (20) is approximated by (21) and the right-hand side of (20) is approximated as $(\varepsilon_r^2\cos^2\theta_s)/(\varepsilon_r - \sin^2\theta_s) \approx \varepsilon_r\cos^2\theta_s$, following inequality is obtained:

$$\sin^2(k_0 h_{(1,\theta_s)}\cos\theta_i) \le \frac{\cos^2\theta_s}{\cos^2\theta_i}. \tag{22}$$

Since ε_r is not included in (22), it is found that the range of the incident angle θ_i for enhancing the scattering field strength of the infinite line current backed by the ground plane with the dielectric superstrate is independent of ε_r when $\varepsilon_r \gg 1$.

IV. Numerical Results

A. Numerical Analysis of Formulae

Effect of the superstrate on the scattering field strength is demonstrated numerically. As mentioned earlier, both of the incident angle θ_i and scattering angle θ_s affect the scattering field strength. In order to clarify the effect of the incident angle θ_i and scattering angle θ_s on the scattering field strength, a following quantity is evaluated:

$$f^{\mathrm{TE/TM}}(\theta_s, \theta_i) = \left|\frac{E_0^{\mathrm{TE/TM}}(\theta_s, a)}{F^{\mathrm{TE/TM}}(\theta_s, h_{(1,\theta_s)}, t_{(1,\theta_s)}, \varepsilon_r)} \times \frac{E_0^{\mathrm{TE/TM}}(\theta_i, a)}{F^{\mathrm{TE/TM}}(\theta_i, h_{(1,\theta_s)}, t_{(1,\theta_s)}, \varepsilon_r)}\right|. \tag{23}$$

Equation (23) is corresponding to the scattering field strength in $\theta = \theta_s$ from the scatterer illuminated by the incident wave arriving from $\theta = \theta_i$. Here, the geometry of the scatterer is designed so that resonance conditions for the scattering angle $\theta = \theta_s$ are satisfied, i.e., $h = h_{(1,\theta_s)}$ and $t = t_{(1,\theta_s)}$. It should be noted that $F^{\mathrm{TE/TM}}$ in (23) is unity for the scatterer without superstrate.

Figs. 2 and 3 is the scattering field strength in $\theta = \theta_s$ from the scatterer illuminated by the plane wave of TE/TM incidence arriving from $\theta = \theta_i$. Here, the scattering field strength is obtained using (23).

According to Fig. 2, it is found that the scattering field strength of the scatterer is higher than that without the superstrate when the incident angle θ_i is in a specific range. Moreover, it is demonstrated that the range of the incident angle θ_i is independent of ϵ_r as predicted from (18). The ranges of the incident angle θ_i predicted by (18) are $\theta_i \le 42.5°$ for $\theta_s = 0$, $\theta_i \le 50.3°$ for $\theta_s = 30°$, and $\theta_i \le 68.3°$ for $\theta_s = 60°$, respectively. It is found that the predicted ranges of θ_i coincide with calculated one using (18).

According to Fig. 3, it is found that the scattering field strength in θ_s can be enhanced by the superstrate when the incident angle θ_i is in a specific range. Although the range of θ_i is almost independent of ε_r for TE incidence, the range of θ_i depends on ε_r for TM incidence when ε_r is a moderate value. However, it is found that the range of θ_i is also independent of ε_r for TM incidence as ε_r becomes large. The ranges of the incident angle θ_i predicted by (22) are $\theta_i \le 90°$ for $\theta_s = 0$, $\theta_i \le 90°$ for $\theta_s = 30°$, and $\theta_i \le 24.8°, \theta_i \ge 50.1°$ for $\theta_s = 60°$, respectively. It is found that the predicted ranges of θ_i coincide with calculated one using (22).

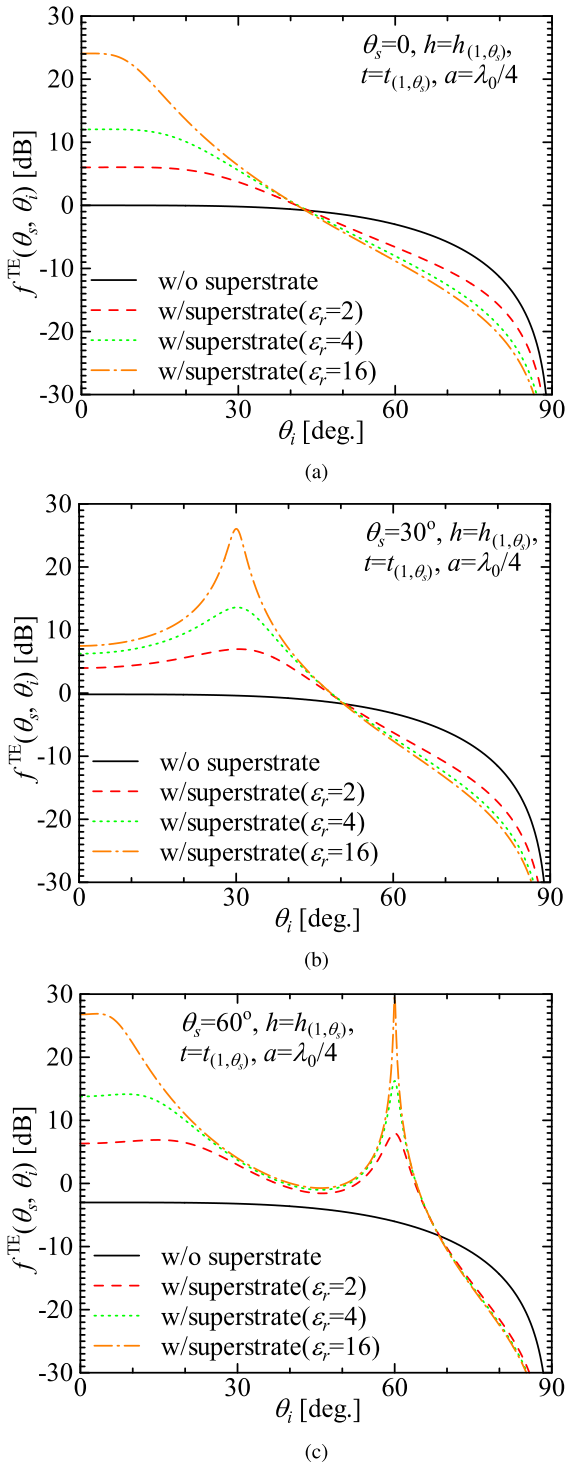

Fig. 2. Scattering field strength (TE incidence). (a) $\theta_s = 0$. (b) $\theta_s = 30°$. (c) $\theta_s = 60°$.

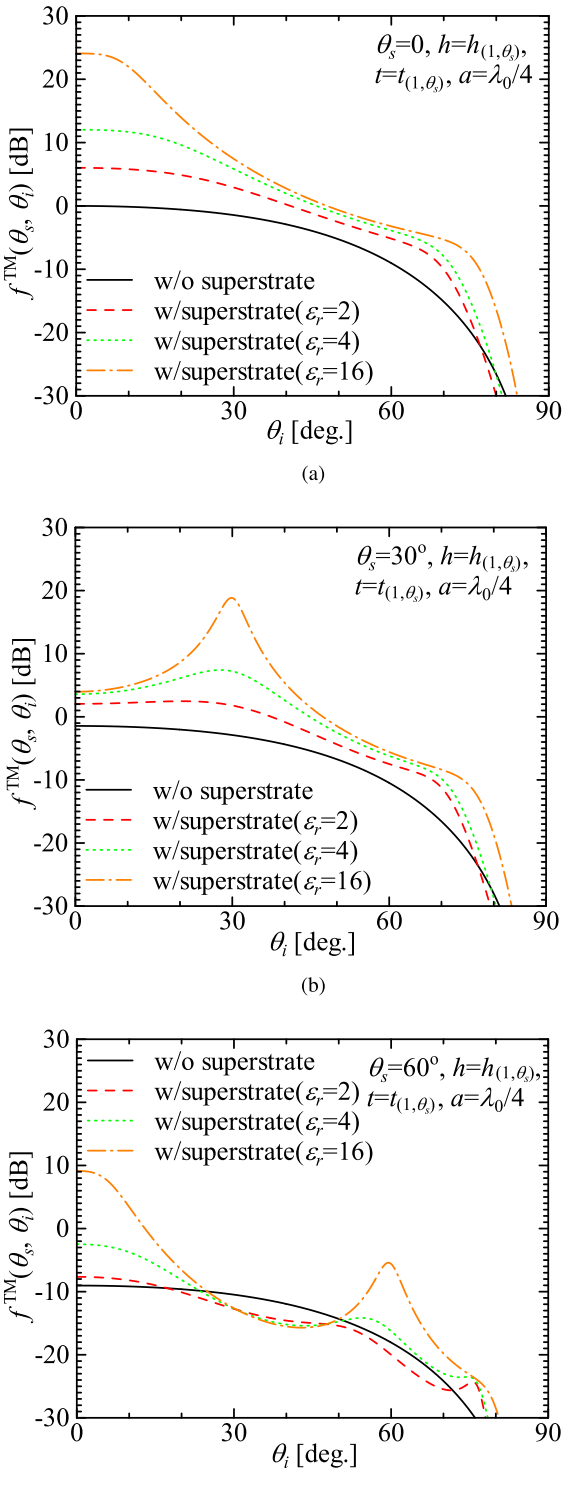

Fig. 3. Scattering field strength (TM incidence). (a) $\theta_s = 0$. (b) $\theta_s = 30°$. (c) $\theta_s = 60°$.

In practical reflectarrays, position of each reflectarray element is different in radial direction. Therefore, the reflectarray elements are illuminated by the incident wave coming from different angle of incidence when the primary source is in a specific position. The effect of the superstrate on the scattering field strength is still expected to be available when the angle of incidence is in the ranges discussed here.

B. Numerical Analysis of Practical Scatterers

As mentioned earlier, the derived formulae and theories are for the infinitely long line current backed by the ground plane with the superstrate. On the other hand, practical reflectarray element is finite size and its geometry is not always linear. Here, the scattering field strength of the various practical

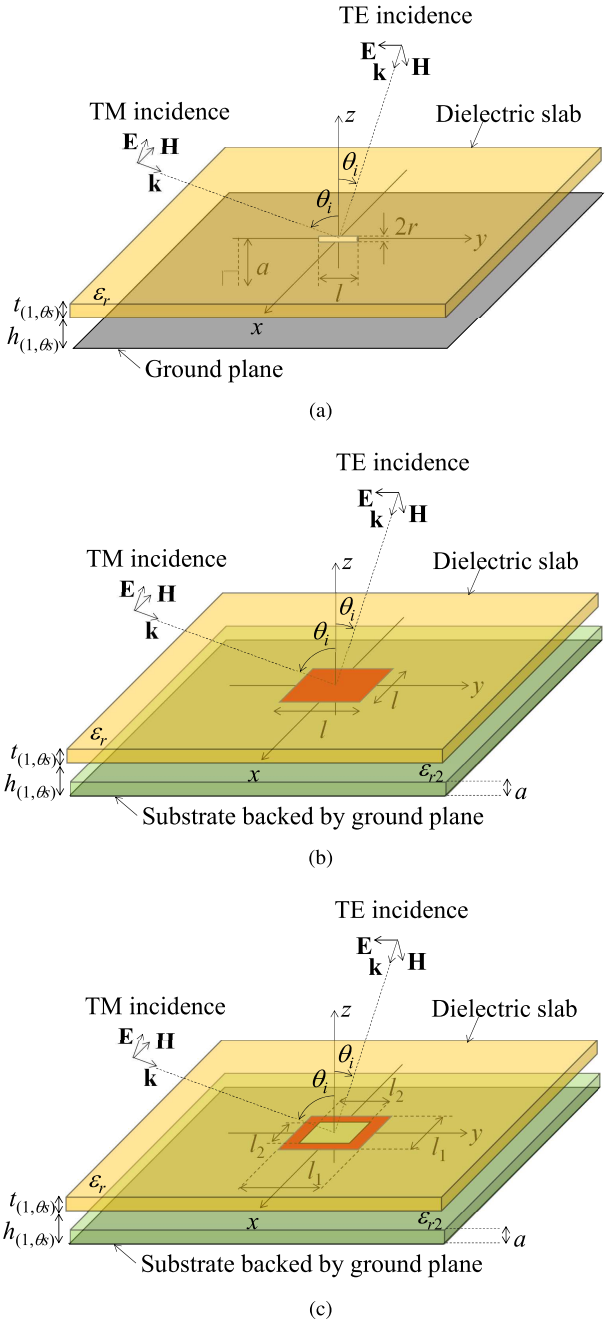

Fig. 4. Numerical analysis models. (a) Dipole element. (b) Patch element. (c) Loop element.

scatterers backed by the ground plane with the superstrate is demonstrated via numerical analysis using MoM.

Fig. 4 shows the examples of the practical scatterers. All of the scatterers are backed by the infinite ground plane and are covered by the infinite dielectric superstrate. Patch and loop elements are on an infinite dielectric substrate. Height and thickness of the superstrate are designed so that resonance condition is satisfied at a specific scattering angle θ_s, i.e., $h = h_{(1,\theta_s)}$ and $t = t_{(1,\theta_s)}$. The scatterers are illuminated by plane wave of TE/TM incidence from $\theta = \theta_i$ and their scattering fields are obtained. Numerical simulation is performed using a commercial simulator software, FEKO.

In order to demonstrate the effect of the superstrate on the scattering field strength, normalized scattering field is evaluated as follows:

$$g^{\mathrm{TE/TM}} = \left| \frac{E_{\mathrm{w}}^{\mathrm{TE/TM}}(\theta_s, \theta_i, h_{(1,\theta_s)}, t_{(1,\theta_s)}, \varepsilon_r)}{E_{\mathrm{w/o}}^{\mathrm{TE/TM}}(\theta_s, \theta_i)} \right| \tag{24}$$

where $E_{\mathrm{w}}^{TE/TM}$ and $E_{\mathrm{w/o}}^{TE/TM}$ are the scattering field of the scatterer with and without superstrate, respectively. Equation (24) indicates that the scattering field strength in $\theta = \theta_s$ is enhanced by the superstrate when $g^{\mathrm{TE/TM}}$ is larger than unity (or 0 dB) and vice versa.

Results of numerical simulation are shown in Figs. 5 and 6. It is found that the effect of the superstrate on the scattering field strength is almost independent of type of the scatterers and just depends on θ_s, θ_i, h, t, ε_r, and polarization of the incident wave. Moreover, Figs. 5 and 6 show that the normalized scattering field strength of the scatterer can be described using (12) and (13) for all types of the scatterers simulated here. For example, it is easily found that $g^{\mathrm{TE/TM}}$ [dB] is coincident with $20\log|\varepsilon_r|$ when $\theta_s = \theta_i = 0$ as shown in Fig. 5(a) and 6(a). According to (3)–(9), the scattering field strength of the scatterer is expressed as a product of the terms corresponding to the effect of the superstrate ($=F^{\mathrm{TE/TM}}$) and the electric field of the scatterer without superstrate ($=E_0^{\mathrm{TE/TM}}$). Since $F^{\mathrm{TE/TM}}$ is completely separated from $E_0^{\mathrm{TE/TM}}$ and is independent of the geometry except for the superstrate, it is expected that $F^{\mathrm{TE/TM}}$ can be applicable for describing the effect of the superstrate on the scattering field strength of the various types of the scatterers. Results of numerical simulation shown in Figs. 5 and 6 have demonstrated the applicability of $F^{\mathrm{TE/TM}}$ to design of various types of the scatterers with the dielectric superstrate.

On the other hand, according to Figs. 5 and 6, it is found that the threshold of θ_i for keeping the normalized scattering field strength over 0 dB is independent of the type of the scatterer and ε_r. For example, according to Fig. 5, the threshold of θ_i for keeping the normalized scattering field strength over 0 dB is within $40^\circ \le \theta_i \le 50^\circ$ for $\theta_s = 0$, $50^\circ \le \theta_i \le 60^\circ$ for $\theta_s = 30^\circ$, and $60^\circ \le \theta_i \le 70^\circ$ for $\theta_s = 60^\circ$, respectively. These numerical results are roughly coincident with those of analytical formulae because thresholds of θ_i obtained from (18) are $\theta_i \approx 42.5^\circ$ for $\theta_s = 0$, $\theta_i \approx 50.3^\circ$ for $\theta_s = 30^\circ$, and $\theta_i \approx 68.3^\circ$ for $\theta_s = 60^\circ$, respectively. Moreover, it should be noted here that the thresholds of θ_i found here are corresponding to intersections between solid black line (w/o superstrate) and the other lines (w/superstrate) shown in Fig. 2(a)–(c). For TM incidence, as shown in Fig. 6, the normalized scattering field strength is over 0 dB for all the incident angle θ_i when $\epsilon_r \gg 1$ and $\theta_s = 0^\circ, 30^\circ$. On the other hand, the normalized scattering field strength at $\theta_s = 60^\circ$ for the plane wave of TM incidence arriving from $30^\circ \le \theta_i \le 50^\circ$ is below 0 dB as shown in Fig. 6(c). These numerical results are roughly coincident with those of analytical formulae because thresholds of θ_i obtained from (22) are $\theta_i \approx 90^\circ$ for $\theta_s = 0$, $\theta_i \approx 90^\circ$ for $\theta_s = 30^\circ$ and $\theta_i \approx 24.8^\circ, \theta_i \approx 50.1^\circ$ for $\theta_s = 60^\circ$, respectively. Moreover, it should be noted here

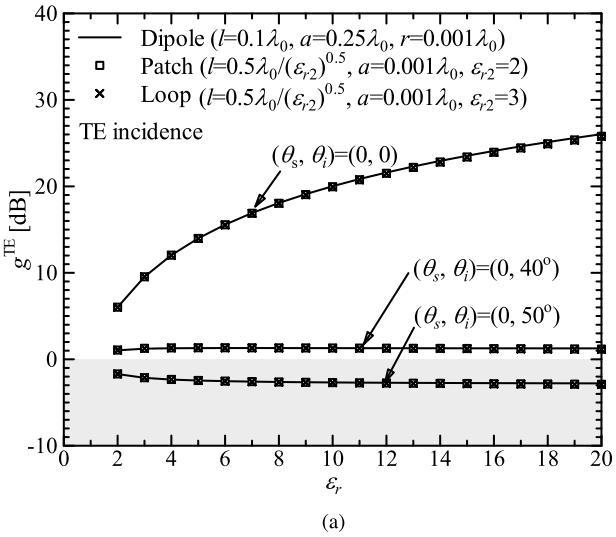

(a)

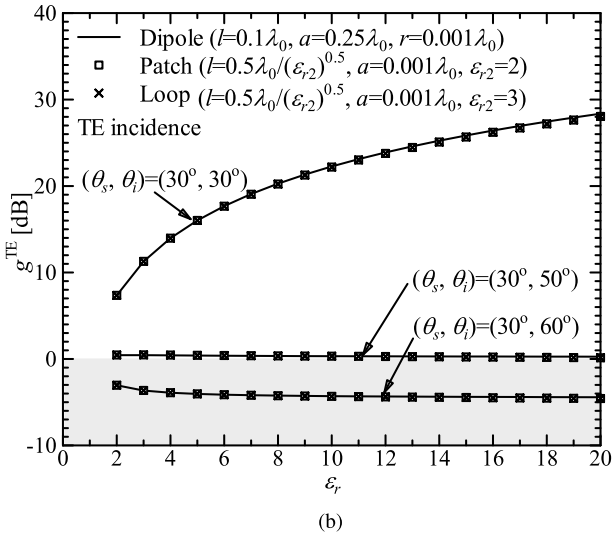

(b)

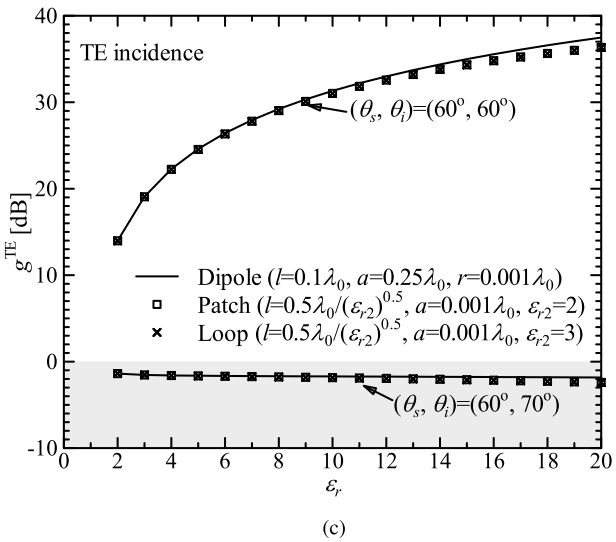

(c)

Fig. 5. Normalized scattering field strength (TE incidence). Colored area indicates that scattering field strength of the scatterer with the dielectric superstrate is lower than that without the dielectric superstrate. (a) $\theta_s = 0$. (b) $\theta_s = 30°$. (c) $\theta_s = 60°$.

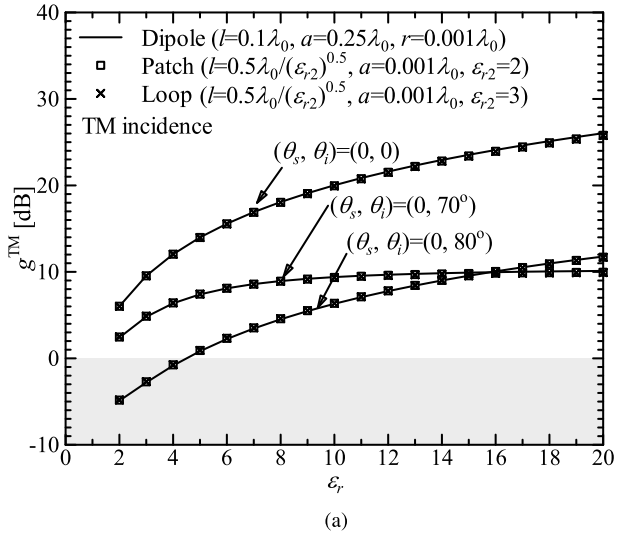

(a)

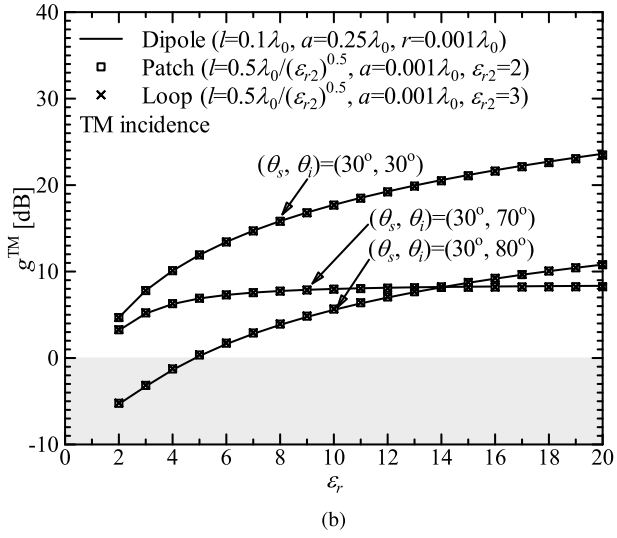

(b)

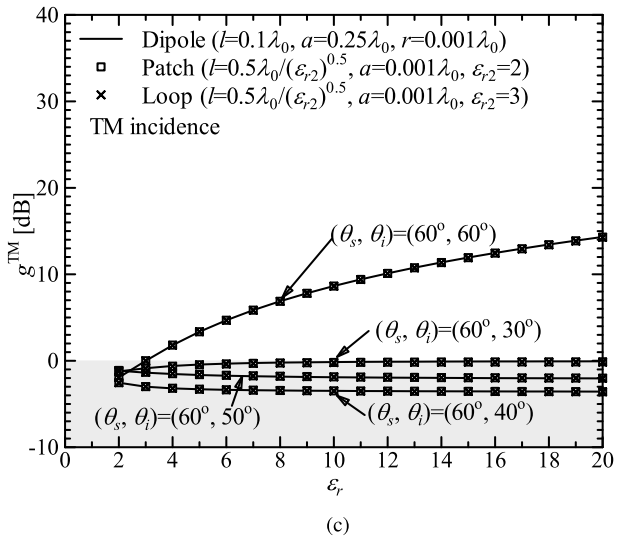

(c)

Fig. 6. Normalized scattering field strength (TM incidence). Colored area indicates that scattering field strength of the scatterer with the dielectric superstrate is lower than that without the dielectric superstrate. (a) $\theta_s = 0$. (b) $\theta_s = 30°$. (c) $\theta_s = 60°$.

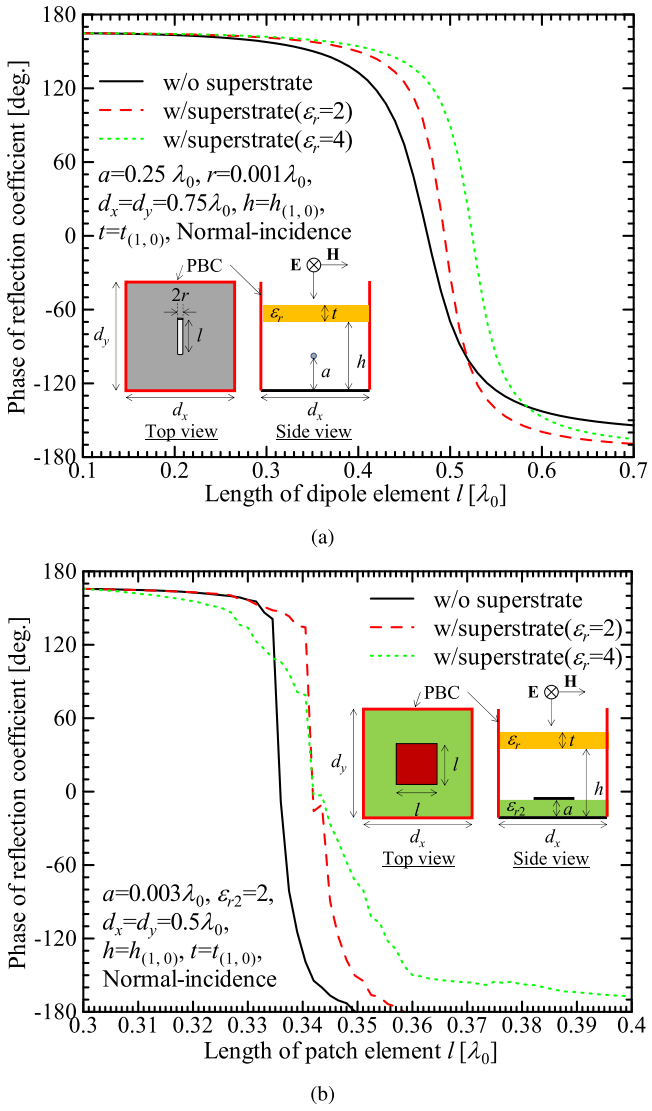

Fig. 7. Phase of reflection coefficient under PBC. (a) Dipole. (b) Patch.

that the thresholds of θ_i found here are corresponding to intersections between solid black line (w/o superstrate) and the other lines (w/superstrate) shown in Fig. 3(a)–(b).

According to these numerical results, it can be concluded that the derived formulae and theories in this article are applicable to design of the various types of scatterers backed by the ground plane with the dielectric superstrate.

Finally, phase of reflection coefficient under the periodic boundary condition (PBC) was obtained in order to demonstrate the effect of the dielectric superstrate on it. Fig. 7 shows the phase of reflection coefficient of the dipole and patch element that is obtained using FEKO. The phase of the reflection coefficient corresponding to the smallest value of l obtained from the scatterers without superstrate is reference value. All of the curves are shifted so that they start from the reference value. Phase shift of the curves is 77° and 151° for the dipole with superstrate whose relative permittivity is $\varepsilon_r = 2, 4$. On the other hand, phase shift of the curves is 304° and 97° for the patch with superstrate whose relative permittivity is $\varepsilon_r = 2, 4$. According to Fig. 7, it is found that the phase of the reflection coefficient is affected by the dielectric superstrate. The dielectric superstrate is expected to affect spatial phase delay because gradient of the phase (i.e., wavenumber) inside the dielectric superstrate is larger than that in free-space. Moreover, current of the scatterers is affected by the mutual coupling between the scatterers and the dielectric superstrate. Effect of the dielectric superstrate on the phase of reflection coefficient can be described qualitatively in this manner. Although the dielectric superstrate affects the phase of reflection coefficient, phase variation approximately ranging from $-180°$ to 180°, which is comparable to that of practical reflectarray elements, is available even when the scatterers are covered by the superstrate. Therefore, it can be concluded that the scatterers covered by the superstrate can be applicable to the reflectarray element.

V. Conclusion

In this article, effect of the superstrate on the scattering field strength of the reflectarray element has been clarified theoretically. At first, the far-field expressions of the infinite line current backed by the ground plane with the dielectric superstrate under the resonance conditions have been reviewed. According to the expressions and reciprocity, it has been demonstrated that the effect of the dielectric superstrate on the scattering field strength is squared when the resonance conditions are satisfied for $\theta = \theta_i = \theta_s$. Moreover, the effect of the incident angle θ_i on the scattering field strength of the infinite line scatterer backed by the ground plane with the dielectric superstrate under the resonance conditions has been clarified. It has been demonstrated that the scattering field strength is enhanced by the dielectric superstrate under the resonance conditions only when the incident angle θ_i is in a specific range. Moreover, it has been found that the range of the incident angle θ_i is independent of ϵ_r when $\epsilon_r \gg 1$. Next, a couple of finite reflectarray elements covered by the dielectric superstrate are modeled and their scattering performances have been simulated using the MoM. It has been demonstrated that the derived theories in this article work for design of the practical reflectarray elements covered by the dielectric superstrate. Finally, the effect of the dielectric superstrate on phase variation of reflection coefficient has been demonstrated numerically. It has been shown that phase variation approximately ranging from $-180°$ to 180° is available and scatterers covered by the superstrate can be applicable to the reflectarray element.

Although this article has focused on the effect of the homogeneous and flat dielectric superstrate, inhomogeneous and nonflat dielectric superstrate may also have a potential to enhance the scattering performance of the reflectarray element. The study of the reflectarray element covered by the inhomogeneous and nonflat dielectric superstrate is beyond the scope of this article and is remaining as a future work.

Results and theories demonstrated in this article contribute to find quantitative guidelines on designing the reflectarray elements covered by the superstrate from the viewpoints of angle dependance, geometry, and permittivity of the superstrate. As a summary, impactful contributions of this work are listed as follows.

1) According to the analytical expressions and reciprocity, effect of the dielectric superstrate on the scattering field strength is squared when the resonance conditions are satisfied for $\theta = \theta_i = \theta_s$.
2) Incident angle of the plane wave for enhancing scattering field strength by the dielectric superstrate is limited in a specific range. The range is obtained from the analytical expressions and is independent of relative permittivity ε_r of the dielectric superstrate when $\epsilon_r \gg 1$.
3) The effect of the dielectric superstrate and incident angle of the plane wave on the scattering field strength derived in this work is available on the practical scatterers.

According to theoretical studies performed in this article, potential application of the dielectric superstrate to enhance the scattering performance of the reflectarray elements has been clarified. This work is a milestone of the reflectarray covered by the dielectric superstrate that are promising technologies for future wireless systems.

REFERENCES

[1] Y. Sugio, T. Makimoto, S. Nishimura, and T. Tsugawa, "Analysis for gain enhancement of multiple-reflection line antenna with dielectric plates," *IEICE Tech. Rep.*, vol. 112, pp. 7–12, Jan. 1981.

[2] Y. Sugio, T. Makimoto, and T. Tsugawa, "Two-dimensional analysis for gain enhancement of dielectric loaded antenna with a ground plane," *Electron. Commun. Japan*, vol. 7, no. 8, pp. 405–412, Aug. 1990.

[3] Y. Sugio, T. Makimoto, and T. Tsugawa, "Two-dimensional analysis for gain enhancement of dielectric loaded antenna with a ground plane," *Electron. Commun. Jpn. I, Commun.*, vol. 74, no. 5, pp. 71–79, May 1991.

[4] N. G. Alexópoulos and D. R. Jackson, "Fundamental superstrate (cover) effects on printed circuit antennas," *IEEE Trans. Antennas Propag.*, vol. AP-32, no. 8, pp. 807–816, Aug. 1984.

[5] D. R. Jackson and N. Alexopoulos, "Gain enhancement methods for printed circuit antennas," *IEEE Trans. Antennas Propag.*, vol. AP-33, no. 9, pp. 976–987, Sep. 1985.

[6] D. Jackson and N. Alexópoulos, "Analysis of planar strip geometries in a substrate-superstrate configuration," *IEEE Trans. Antennas Propag.*, vol. AP-34, no. 12, pp. 1430–1438, Dec. 1986.

[7] H. Yang and N. Alexópoulos, "Gain enhancement methods for printed circuit antennas through multiple superstrates," *IEEE Trans. Antennas Propag.*, vol. AP-35, no. 7, pp. 860–863, Jul. 1987.

[8] D. R. Jackson, "The RCS of a rectangular microstrip patch in a substrate-superstrate geometry," *IEEE Trans. Antennas Propag.*, vol. 38, no. 1, pp. 2–8, Jan. 1990.

[9] J. C. Iriarte *et al.*, "EBG superstrate array configuration for the WAAS space segment," *IEEE Trans. Antennas Propag.*, vol. 57, no. 1, pp. 81–93, Jan. 2009.

[10] A. Foroozesh and L. Shafai, "Effects of artificial magnetic conductors in the design of low-profile high-gain planar antennas with high-permittivity dielectric superstrate," *IEEE Antennas Wireless Propag. Lett.*, vol. 8, pp. 10–13, 2009.

[11] Z.-H. Wu and W.-X. Zhang, "Broadband printed compound air-fed array antennas," *IEEE Antennas Wireless Propag. Lett.*, vol. 9, pp. 187–190, 2010.

[12] R. Guzman-Quiros, J. L. Gomez-Tornero, A. R. Weily, and Y. J. Guo, "Electronically steerable 1-D Fabry–Perot leaky-wave antenna employing a tunable high impedance surface," *IEEE Trans. Antennas Propag.*, vol. 60, no. 11, pp. 5046–5055, Nov. 2012.

[13] A. Ghasemi, S. N. Burokur, A. Dhouibi, and A. de Lustrac, "High beam steering in Fabry–Pérot leaky-wave antennas," *IEEE Antennas Wireless Propag. Lett.*, vol. 12, pp. 261–264, 2013.

[14] D. Germain, D. Seetharamdoo, S. N. Burokur, and A. de Lustrac, "Thin conformal directive Fabry–Pérot cavity antenna," *IEEE Antennas Wireless Propag. Lett.*, vol. 12, pp. 926–929, 2013.

[15] F. Meng and S. K. Sharma, "A dual-band high-gain resonant cavity antenna with a single layer superstrate," *IEEE Trans. Antennas Propag.*, vol. 63, no. 5, pp. 2320–2324, May 2015.

[16] J. H. Kim, C.-H. Ahn, and J.-K. Bang, "Antenna gain enhancement using a holey superstrate," *IEEE Trans. Antennas Propag.*, vol. 64, no. 3, pp. 1164–1167, Mar. 2016.

[17] F. Sultan and S. S. I. Mitu, "Superstrate-based beam scanning of a Fabry–Perot cavity antenna," *IEEE Antennas Wireless Propag. Lett.*, vol. 15, pp. 1187–1190, 2016.

[18] P. Xie, G. Wang, H. Li, and J. Liang, "A dual-polarized two-dimensional beam-steering Fabry–Pérot cavity antenna with a reconfigurable partially reflecting surface," *IEEE Antennas Wireless Propag. Lett.*, vol. 16, pp. 2370–2374, 2017.

[19] F. Scattone, M. Ettorre, B. Eddo, R. Sauleau, and N. J. G. Fonseca, "Truncated leaky-wave antenna with cosecant-squared radiation pattern," *IEEE Antennas Wireless Propag. Lett.*, vol. 17, no. 5, pp. 841–844, May 2018.

[20] A. T. Almutawa, A. Hosseini, D. R. Jackson, and F. Capolino, "Leaky-wave analysis of wideband planar Fabry–Pérot cavity antennas formed by a thick PRS," *IEEE Trans. Antennas Propag.*, vol. 67, no. 8, pp. 5163–5175, Aug. 2019.

[21] D. Berry, R. Malech, and W. Kennedy, "The reflectarray antenna," *IEEE Trans. Antennas Propag.*, vol. AP-11, no. 6, pp. 645–651, Nov. 1963.

[22] J. Huang, "Analysis of a microstrip reflectarray antenna for microspacecraft applications," Jet Propuls. Lab., NASA, Washington, DC, USA, TDA Prog. Rep. 42-120, Feb. 1995, pp. 153–173.

[23] J. Huang and J. A. Encinar, *Reflectarray Antennas*. Hoboken, NJ, USA: Wiley, 2008.

[24] F. Venneri, G. Angiulli, and G. Di Massa, "Design of microstrip reflect array using data from isolated patch analysis," *Microw. Opt. Technol. Lett.*, vol. 34, no. 6, pp. 411–414, Sep. 2002.

[25] M.-A. Milon, D. Cadoret, R. Gillard, and H. Legay, "'Surrounded-element' approach for the simulation of reflectarray radiating cells," *IET Microw., Antennas Propag.*, vol. 1, no. 2, pp. 289–293, Apr. 2007.

[26] C. Yann, R. Loison, R. Gillard, M. Labeyrie, and J. P. Martinaud, "A new approach combining surrounded-element and compression methods for analyzing reconfigurable reflectarray antennas," *IEEE Trans. Antennas Propag.*, vol. 60, no. 7, pp. 3215–3221, Jul. 2012.

[27] K. Konno and Q. Chen, "Enhancing aperture efficiency of reflectarray by accurately evaluating mutual coupling of reflectarray elements," *IEICE Commun. Exp.*, vol. 5, no. 9, pp. 341–346, 2016.

[28] T. Susuga, K. Konno, and Q. Chen, "A study on fast method of moments for large-scale reflectarrays," in *Proc. ICETC*, Dec. 2020, p. 1.

[29] P. Nayeri *et al.*, "3D printed dielectric reflectarrays: Low-cost high-gain antennas at sub-millimeter waves," *IEEE Trans. Antennas Propag.*, vol. 62, no. 4, pp. 2000–2008, Apr. 2014.

[30] K. Yokokawa, K. Konno, and Q. Chen, "Scattering performance of log-periodic dipole array," *IEEE Antennas Wireless Propag. Lett.*, vol. 16, pp. 740–743, 2017.

[31] H. Ito, K. Konno, H. Sato, and Q. Chen, "Wideband scattering performance of reflectarray using log-periodic dipole array," *IEEE Antennas Wireless Propag. Lett.*, vol. 16, pp. 1305–1308, 2017.

[32] K. Konno, H. Sato, Q. Chen, and H. Itoh, "Scattering performance of a reflectarray using log-periodic dipole array element," in *Proc. Int. Symp. Antennas Propag. (ISAP)*, Oct. 2017, pp. 1–2.

[33] K. Konno and Q. Chen, "A reflectarray using log-periodic dipole array element," in *IEEE MTT-S Int. Microw. Symp. Dig.*, May 2018, pp. 1–3.

[34] K. Konno, Q. Yuan, and Q. Chen, "Ninja array antenna: Novel approach for low backscattering phased array antenna," *IET Microw., Antennas Propag.*, vol. 12, no. 3, pp. 346–353, Feb. 2018.

[35] M. D. Wu *et al.*, "Design and measurement of a 220 GHz wideband 3-D printed dielectric reflectarray," *IEEE Antennas Wireless Propag. Lett.*, vol. 17, no. 11, pp. 2094–2098, Nov. 2018.

[36] K. Konno, Q. Chen, and Q. Yuan, "Scattering and radiation performance of ninja array antennas," in *Proc. Asia–Pacific Microw. Conf. (APMC)*, Nov. 2018, pp. 1–3.

[37] G. Wu, Y. S. Zeng, K. F. Chan, B. J. Chen, S. W. Qu, and C. H. Chan, "High-gain filtering reflectarray antenna for millimeter-wave applications," *IEEE Trans. Antennas Propag.*, vol. 68, no. 2, pp. 805–812, Feb. 2020.

[38] D. Pilz and W. Menzel, "Folded reflectarray antenna," *Electron. Lett.*, vol. 34, no. 9, pp. 832–833, Apr. 1988.

[39] W. Menzel, D. Pilz, and M. Al-Tikriti, "Millimeter-wave folded reflector antennas with high gain, low loss, and low profile," *IEEE Antennas Propag. Mag.*, vol. 44, no. 3, pp. 24–29, Jun. 2002.

[40] J. A. Zornoza, R. Leberer, J. A. Encinar, and W. Menzel, "Folded multilayer microstrip reflectarray with shaped pattern," *IEEE Trans. Antennas Propag.*, vol. 54, no. 2, pp. 510–518, Feb. 2006.

[41] A. Zeitler, J. Lanteri, C. Pichot, C. Migliaccio, P. Feil, and W. Menzel, "Folded reflectarrays with shaped beam pattern for foreign object debris detection on runways," *IEEE Trans. Antennas Propag.*, vol. 58, no. 9, pp. 3065–3068, Sep. 2010.

[42] J. Ren and W. Menzel, "Dual-frequency folded reflectarray antenna," *IEEE Antennas Wireless Propag. Lett.*, vol. 12, pp. 1216–1219, 2013.

[43] M. Jiang, W. Hong, Y. Zhang, S. H. Yu, and H. Zhou, "A folded reflectarray antenna with a planar SIW slot array antenna as the primary source," *IEEE Trans. Antennas Propag.*, vol. 62, no. 7, pp. 3575–3583, Jul. 2014.

[44] L. Guo, P.-K. Tan, and T.-H. Chio, "On the use of single-layered subwavelength rectangular patch elements for broadband folded reflectarrays," *IEEE Antennas Wireless Propag. Lett.*, vol. 16, pp. 424–427, 2017.

[45] J. Yang, Y. Shen, L. Wang, H. Meng, W. Dou, and S. Hu, "2-D scannable 40-GHz folded reflectarray fed by SIW slot antenna in single-layered PCB," *IEEE Trans. Microw. Theory Techn.*, vol. 66, no. 6, pp. 3129–3135, Jun. 2018.

[46] J. Yang, Q. Cheng, M. K. T. Al-Nuaimi, A. Kishk, and A.-E. Mahmoud, "Broadband folded reflectarray fed by a dielectric resonator antenna," *IEEE Antennas Wireless Propag. Lett.*, vol. 19, no. 1, pp. 178–182, Jan. 2020.

[47] Y. Cao, W. Che, W. Yang, C. Fan, and Q. Xue, "Novel wideband polarization rotating metasurface element and its application for wideband folded reflectarray," *IEEE Trans. Antennas Propag.*, vol. 68, no. 3, pp. 2118–2127, Mar. 2020.

[48] A. Freni, A. Mazzinghi, and G. Carluccio, "Folded reflectarray with spherical polarizer," *IEEE Trans. Antennas Propag.*, vol. 68, no. 5, pp. 3613–3624, May 2020.

[49] X.-C. Zhu, P.-P. Zhang, Y.-X. Zhang, J.-X. Ge, and Z.-H. Gao, "A high-gain filtering antenna based on folded reflectarray antenna and polarization-sensitive frequency selective surface," *IEEE Antennas Wireless Propag. Lett.*, vol. 19, no. 8, pp. 1462–1465, Aug. 2020.

[50] Z. Wang *et al.*, "1 bit electronically reconfigurable folded reflectarray antenna based on p-i-n diodes for wide-angle beam-scanning applications," *IEEE Trans. Antennas Propag.*, vol. 68, no. 9, pp. 6806–6810, Sep. 2020.

[51] S. M. Meriah, E. Cambiaggio, R. Staraj, and F. T. Bendimerad, "Gain enhancement for microstrip reflectarray using superstrate layer," *Microw. Opt. Technol. Lett.*, vol. 46, no. 2, pp. 152–154, Jul. 2005.

Keisuke Konno (Member, IEEE) received the B.E., M.E., and D.E. degrees from Tohoku University, Sendai, Japan, in 2007, 2009, and 2012, respectively.

Since 2012, he has been with the Department of Communications Engineering, Graduate School of Engineering, Tohoku University, where he is currently an Associate Professor. He was with the ElectroScience Laboratory, The Ohio State University, Columbus, OH, USA, as a Visiting Scholar, from 2015 to 2017. His research interests include computational electromagnetics, array antennas, reflectarrays, and source reconstruction.

Dr. Konno is a member of the Institute of Electronics, Information and Communication Engineers (IEICE). He received the JSPS Postdoctoral Fellowships for Research Abroad. He received the Encouragement Award for Young Researcher and the Most Frequent Presentations Award in 2010 from the Technical Committee on Antennas and Propagation of Japan, the Young Researchers Award in 2011 from IEICE of Japan, the IEEE EMC Society Sendai Chapter Student Brush-up Session and the EMC Sendai Seminar Student Best Presentation Award in 2011, the Japan Society for the Promotion of Science (JSPS) Washington Director Award in 2016, the MHz Rectenna Award in 2017, the Young Researchers Award for Electrical Engineering, Communication Engineering, Electronic Engineering, Information Engineering (ECEI) of Tohoku University in 2018, the Minoru Ishida Award in 2018, the IEEE AP-S Japan Young Engineer Award in 2018, the TOKIN Foundation Research Encouragement Award in 2019, and the IEICE Communications Society Distinguished Contributions Awards in 2019 and 2021.

Qiang Chen (Senior Member, IEEE) received the B.E. degree from Xidian University, Xi'an, China, in 1986, and the M.E. and D.E. degrees from Tohoku University, Sendai, Japan, in 1991 and 1994, respectively.

He is currently a Chair Professor with the Electromagnetic Engineering Laboratory, Department of Communications Engineering, Faculty of Engineering, Tohoku University. His primary research interests include antennas, microwave and millimeter wave, electromagnetic measurement, and computational electromagnetics.

Prof. Chen is a fellow of the Institute of Electronics, Information and Communication Engineers (IEICE). He received the Best Paper Award and the Zen-ichi Kiyasu Award from IEICE. He served as the Chair for IEICE Technical Committee on Photonics-Applied Electromagnetic Measurement from 2012 to 2014, the IEICE Technical Committee on Wireless Power Transfer from 2016 to 2018, the IEEE Antennas and Propagation Society Tokyo Chapter from 2017 to 2018, and the IEICE Technical Committee on Antennas and Propagation from 2019 to 2021.